TTBK2 controls cilium stability by regulating distinct modules of centrosomal proteins

Abraham Nguyen[ORCID],[a,b] and Sarah C. Goetz[ORCID],[b,*]
[a]Molecular Cancer Biology Program and [b]Department of Pharmacology and Cancer Biology, Duke University School of Medicine, Durham, NC 27710

ABSTRACT The serine-threonine kinase tau tubulin kinase 2 (TTBK2) is a key regulator of the assembly of primary cilia, which are vital signaling organelles. TTBK2 is also implicated in the stability of the assembled cilium through mechanisms that remain to be defined. Here we use mouse embryonic fibroblasts derived from *Ttbk2$^{fl/fl}$, UBC-CreERT+* embryos (hereafter *Ttbk2^{cmut}*) to dissect the role of TTBK2 in cilium stability. This system depletes TTBK2 levels after cilia formation, allowing us to assess the molecular changes to the assembled cilium over time. As a consequence of *Ttbk2* deletion, the ciliary axoneme is destabilized and primary cilia are lost within 48–72 h following recombination. Axoneme destabilization involves an increased frequency of cilia breaks and a reduction in axonemal microtubule modifications. Cilia loss was delayed by using inhibitors that affect actin-based trafficking. At the same time, we find that TTBK2 is required to regulate the composition of the centriolar satellites and to maintain the basal body pools of intraflagellar transport proteins. Altogether, our results reveal parallel pathways by which TTBK2 maintains cilium stability.

INTRODUCTION

Primary cilia are critical regulators of a variety of different cell signaling pathways, including Sonic hedgehog and G-protein-coupled receptor (GPCR) signaling (Goetz and Anderson, 2010; Hilgendorf *et al.*, 2016). While most vertebrate cell types have a primary cilium, these structures are dynamic and are assembled and disassembled during development in response to cell cycle as well as extracellular cues (Sánchez and Dynlacht, 2016). While there has been progress in uncovering key players and molecular steps involved in primary cilium assembly, less is known about the regulation of cilium disassembly, or the molecular players and pathways governing stability and maintenance of the assembled ciliary axoneme. Defining the regulation of cilia at each distinct phase of the cilia lifecycle is impor-

tant for our understanding of how critical signal transduction pathways are regulated.

Cilium assembly is initiated at the mother centriole, the older of the cell's two centrioles, which is distinguished from the daughter centriole by the presence of subdistal and distal appendages (DA). These appendages are important for organizing microtubules and for recruiting the machinery that will assemble the cilium, respectively (Bowler *et al.*, 2019). DA proteins including CEP164 are sequentially recruited to the mother centriole (Tanos *et al.*, 2013) downstream of the distal centriolar protein oral-facial-digital-1 (OFD1) (Singla *et al.*, 2010) and in turn mediate the recruitment of the ciliary kinase tau tubulin kinase 2 (TTBK2) as well as ciliary

vesicles that will ultimately give rise to the ciliary membrane (Tanos et al., 2013; Čajánek and Nigg, 2014). Intraflagellar transport (IFT) proteins are then recruited to assemble the cilium by trafficking tubulin and other proteins to assemble the ciliary axoneme which will project from the cell surface (Craft et al., 2015; Nakayama and Katoh, 2018).

In previous studies, we identified a requirement for TTBK2 in the initial stages of cilium assembly, showing that TTBK2 is required both to recruit IFT proteins to the basal body and to remove suppressors of cilium assembly such as CP110 (Goetz et al., 2012). Thus in cultured cells and mouse embryos lacking TTBK2, cilium assembly fails, resulting in midgestation lethality (Goetz et al., 2012). Using a mouse allelic series for *Ttbk2*, we subsequently demonstrated that this kinase is also important for the structure and stability of the ciliary axoneme and for ciliary trafficking (Bowie et al., 2018). Furthermore, deletion of *Ttbk2* in adult mice results in reduced cilia frequency, suggesting that TTBK2 is required to maintain the structure of cilia as well as to initiate its assembly (Bowie and Goetz, 2020). However, the precise mechanisms by which TTBK2 regulates cilium maintenance remain largely unknown.

In this work, we inducibly delete *Ttbk2* from cells in culture to probe its roles in cilium stability. We show that *Ttbk2* deletion leads to progressive cilium instability and an increased frequency of primary cilia fragmentation leading to cilia loss. This cilia loss is partially attenuated by small molecule inhibitors affecting actin-based trafficking. Furthermore, *Ttbk2* deletion results in dysregulation of a distinct set of proteins that localize to or near the centrosome including the loss of IFT pools, and changes in the centriolar satellite composition. This study reveals new molecular roles for TTBK2 in the maintenance of primary cilia integrity and new insights into requirements for primary cilia stability.

RESULTS
Inducible genetic removal of TTBK2 results in ciliary breakage and loss
TTBK2 is recruited to the basal body by DA proteins, where it is essential for early steps of cilium initiation. TTBK2 then remains at the basal body following the completion of ciliary axoneme assembly but is lost from this compartment upon readdition of serum to induce ciliary disassembly (Goetz et al., 2012). Deletion of *Ttbk2* from adult tissues results in loss of cilia (Bowie and Goetz, 2020), implying that TTBK2 might be continuously required at the basal body to promote ciliary trafficking and/or stability. Our analysis of *Ttbk2* hypomorphic mutants identified structural abnormalities in the cilia of cells with reduced levels of TTBK2 protein (Bowie et al., 2018).

To investigate the cellular requirements for TTBK2 in regulating primary cilia stability, we employed mouse embryonic fibroblasts (MEFs) derived from *Ttbk2fl/fl* embryos also expressing a tamoxifen (Tmx)-inducible Cre recombinase under the control of the ubiquitin C promoter (*UBC-CreERT2+*) to allow for genetic removal of *Ttbk2* under temporal control. In the absence of Tmx, these cells, like other fibroblasts, form cilia when cultured in low-serum (0.5% fetal bovine serum [FBS]) conditions, and the percentage of ciliated cells is indistinguishable from WT MEFs (Supplemental Figure S1A). *Ttbk2cmut* MEFs were then cultured in low-serum media for 15 h to induce cilia formation and treated with Tmx (1 µm) to induce Cre-mediated recombination or with the vehicle (Veh), ethanol, as a control. T0 is defined as the point at which Tmx was administered. Tmx- and Veh-treated cells were imaged 0, 24, 48, and 72 h following Tmx treatment (Figure 1A). We found that TTBK2 protein was reduced at the mother centriole within 24–48 h post-Tmx treatment (Figure 1B), as is *Ttbk2* mRNA measured by qPCR (Supplemental

Figure S1B). Cilia frequency was comparable in the Tmx-treated cells relative to Veh-treated for the first 24 h (66.244 ± 4.705% vs. 72.891 ± 5.258 %). By 48 h, cilia frequency in Tmx-treated cells was less than half that of Veh-treated cells (29.66% ± 2.662% vs. 70.00% ± 3.46%) and cilia were nearly gone (10.989 ± 2.549% vs 71.299 ± 3.213%) in the Tmx-treated cells 72 h following treatment with Tmx (Figure 1C). Treatment of *Ttbk2fl/fl*, *UBC-CreERT2*-negative cells with Tmx did not cause loss of cilia, confirming that the cilia loss was not an artifact of Tmx treatment (Supplemental Figure S1C). Stable expression of TTBK2-GFP in Tmx-treated *Ttbk2cmut* MEFs rescued cilia loss, confirming that this is due to specific loss of TTBK2 (Supplemental Figure S1D). Thus this system recapitulates the requirements we have previously identified for TTBK2 in initiating cilium assembly (Goetz et al., 2012) and stability (Bowie et al., 2018).

Having established an inducible system to specifically interrogate the cellular and molecular role of TTBK2 in ciliary stability, we next used this system for live-cell imaging. To follow cilia in real time in the *Ttbk2cmut* MEFs ± Tmx, we crossed *Ttbk2cmut* mice to a double transgenic line expressing *Arl13b-mCherry* and *Centrin2-GFP* (*ACCG* mice) (Higginbotham et al., 2004; Bangs et al., 2015; Loukil et al., 2021) and derived MEFs from *Ttbk2cmut;ACCG* embryos. We verified that loss of cilia in *Ttbk2cmut;ACCG* MEFs treated with Tmx takes place in the same overall time frame as described for *Ttbk2cmut* cells (Supplemental Figure S1E). Given the sharp change in the frequency of ciliated cells from 24 to 48 h and from 48 to 72 h, we performed live-cell imaging in a 20-h window within these critical periods, 30–50 h following treatment of the cells with Veh or Tmx (Supplemental Videos S1–S3). Analysis of these live-imaging studies revealed that the cilia of *Ttbk2cmut;ACCG* cells treated with Tmx underwent frequent breakages (Figure 2A). A small percentage of Veh-treated cells (5.44%) exhibited breakages from the distal tip of the cilium resembling vesicles (referred to as "budding"), whereas about a third of Tmx-treated *Ttbk2cmut;ACCG* cells (29.18%) had one or more such budding events (Figure 2B). Larger fractions of the axoneme- fragments that were larger than a vesicle ranging from a third of the axoneme to the entire axoneme itself- could also be seen breaking off the cilia (33.18%, referred to as "axonemal") in Tmx-treated *Ttbk2cmut;ACCG* cells, whereas no Veh-treated cells exhibited such breakages (Figure 2, A and B). The net result of this is that fewer than half of the observed cilia in our live-imaged *Ttbk2cmut* cells + Tmx were free of axonemal breakages or budding throughout the time filmed in contrast with more than 90% of the control cells. Moreover, we observed an average of nearly 20% of cilia lost entirely from breakages during the period of our movies in Tmx-treated *Ttbk2cmut* cells compared with none for Veh-treated cells (Figure 2C). Therefore our data suggest that TTBK2 maintains cilia by limiting cilia fragmentation.

TTBK2 partially maintains cilium stability by regulating actin dynamics and axonemal microtubules
Our live-imaging results were reminiscent of primary cilia shedding induced by serum stimulation (Mirvis et al., 2019) and suggested that TTBK2 may prevent breakages of the ciliary axoneme, either by promoting recruitment or retention of factors that stabilize the cilium, or by suppressing negative regulators that might promote ciliary disassembly. To address these nonmutually exclusive possibilities, we examined proteins important for stabilizing the ciliary axoneme and those that promote cilium disassembly. We examined several known regulators of cilium disassembly including phosphorylated, active AURKA, PLK1, and KIF2A (Wang et al., 2013; Miyamoto et al., 2015; Loskutov et al., 2018) in the *Ttbk2cmut* cells and did not observe any accumulation of these proteins at the basal
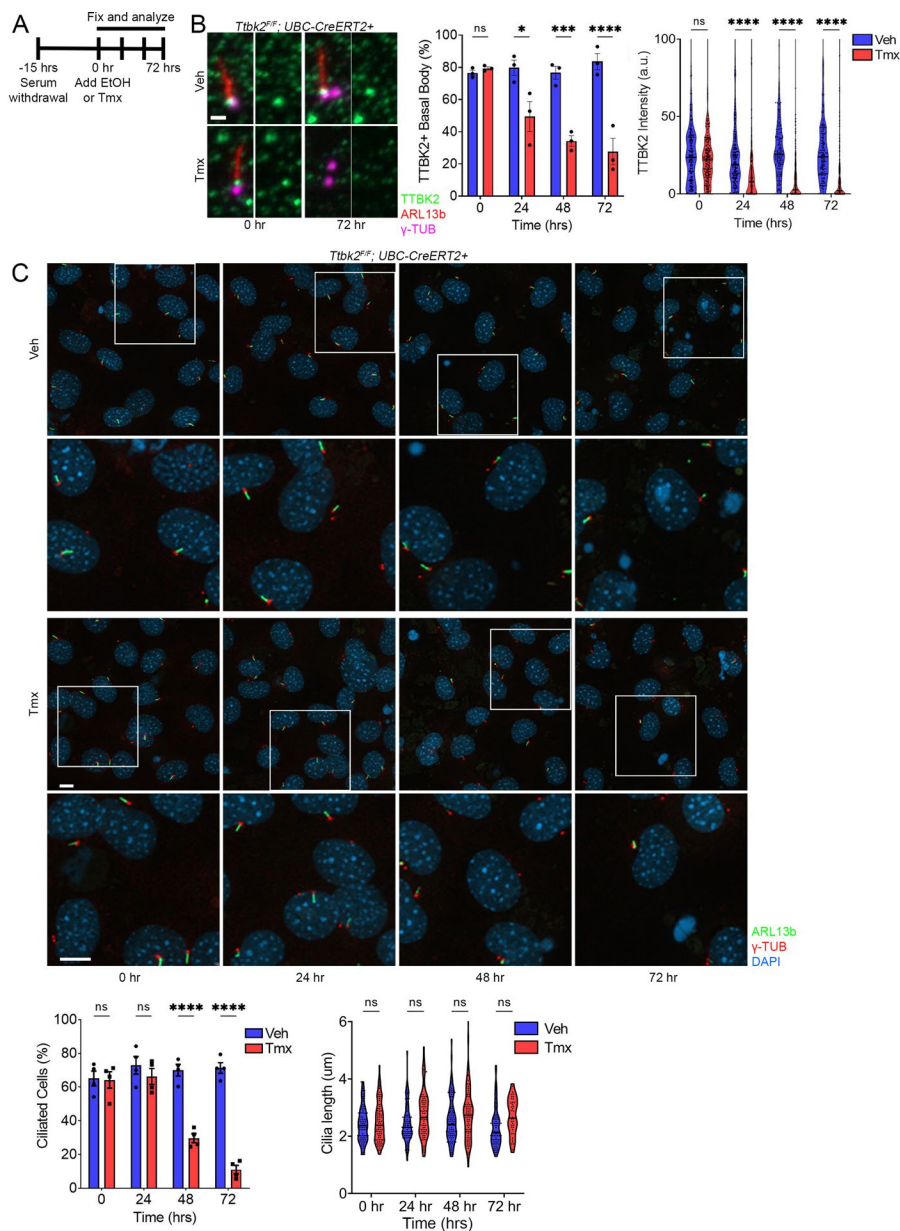
FIGURE 1: TTBK2 is required for maintaining primary cilia. (A) Schematic of experimental design. *Ttbk2fl/fl; UBC-CreERT2+* MEFs were serum-starved for 15 h before being treated with Veh (ethanol) or Tmx. MEFs were then fixed at the indicated time points. (B) Representative images of *Ttbk2fl/fl; UBC-CreERT2+* MEFs treated with Veh or Tmx for 0 and 72 h and immunostained for TTBK2 (green), ARL13b (red), and γ-tubulin (magenta). Scale bar: 1 μm. The graph depicts the mean percentage of basal bodies with positive TTBK2 staining in *Ttbk2fl/fl; UBC-CreERT2+* MEFs after treatment with Veh or Tmx for the indicated durations. Each dot represents an experiment with >50 cells. Statistical comparison was performed by two-way ANOVA with Tukey's multiple comparisons test, *$p < 0.05$, ***$p < 0.001$, ****$p < 0.0001$. Violin plot depicts TTBK2 intensity at the basal body. Results are pooled from three independent experiments. Each dot represents a single measurement ($n > 156$). Statistical comparison was performed by two-way ANOVA with Tukey's multiple comparisons test, ****$p < 0.0001$. (C) Representative images of *Ttbk2fl/fl; UBC-CreERT2+* MEFs treated with Veh or Tmx for 0, 24, 48, and 72 h and stained for ARL13b (green), γ-tubulin (red), and DAPI (blue). Insets are boxed, and magnifications are below their corresponding images. Scale bars: 10 μm. The graph depicts the mean percentage of ciliated cells ± SEM. Each dot represents an experiment with >50 cells. Statistical comparison was performed by two-way ANOVA with Tukey's multiple comparisons test, ****$p < 0.0001$.

body or centrosome following loss of TTBK2 (Supplemental Figure S2, A–C), suggesting that TTBK2 regulates ciliary stability primarily through alternative mechanisms.

A major player in ciliary axonemal stability are microtubules. Specifically, the microtubules that comprise the ciliary axoneme are highly modified, particularly by acetylation and polyglutamylation, and these modifications ensure axonemal stability (He *et al.*, 2020). Because we saw fragments of the axoneme of variable lengths breaking away from cilia, we assessed whether loss of these post-translational modifications could explain how these cilia are destabilized by loss of TTBK2. We found that while tubulin acetylation in the remaining cilia of the *Ttbk2cmut* cells was unaltered at 72 h post-Tmx (Figure 3, A and B), polyglutamylation was substantially reduced relative to control cells both in terms of the extent of polyglutamylated tubulin along the axoneme and staining intensity (Figure 3, A, C, and D). This is consistent with our previous findings for *Ttbk2* hypomorphic mutants (Bowie *et al.*, 2018) and correlates with cilia loss in our conditional mutant cells (Supplemental Figure S2D), implying that TTBK2 plays a role in ensuring that the axonemal microtubules are polyglutamylated, which may in turn confer stability to cilia.

In addition to undermodification of tubulin being associated with instability of the ciliary axoneme (He *et al.*, 2014), alterations to actin dynamics are also linked to ciliary breakage and shedding (Nager *et al.*, 2017; Loukil *et al.*, 2021). We therefore tested several small molecule inhibitors that modulate specific regulators of cytoskeletal dynamics for their ability to affect the phenotype of *Ttbk2cmut* cells treated with Tmx either with respect to the timing or the severity of cilia loss. These drugs included the inhibitors 3,5-bis(trifluoromethyl) pyrazole (BTP2, a drebrin inhibitor) (Mancini *et al.*, 2011), blebbistatin (a myosin II inhibitor) (Shu *et al.*, 2005), Tubastatin A (TBSA, an HDAC6 inhibitor), 2,4,6 Triiodophenol (TIP, a myosin VI inhibitor), and cytochalasin D (CytoD, an actin polymerization inhibitor). In these experiments, we used a similar scheme to that used for our evaluation of cilia loss in *Ttbk2cmut* cells: cells were cultured in low-serum media for 15 h to induce cilium assembly, followed by treatment of the cells with Tmx or Veh to induced Cre-mediated recombination and with the indicated drugs or DMSO Veh (Figure 4A), with the start of Tmx/drug treatment defined as T0. We assessed the proportion of ciliated cells at 48 h, since this is the time point when cilia are appreciably diminished in frequency in *Ttbk2cmut* cells + Tmx
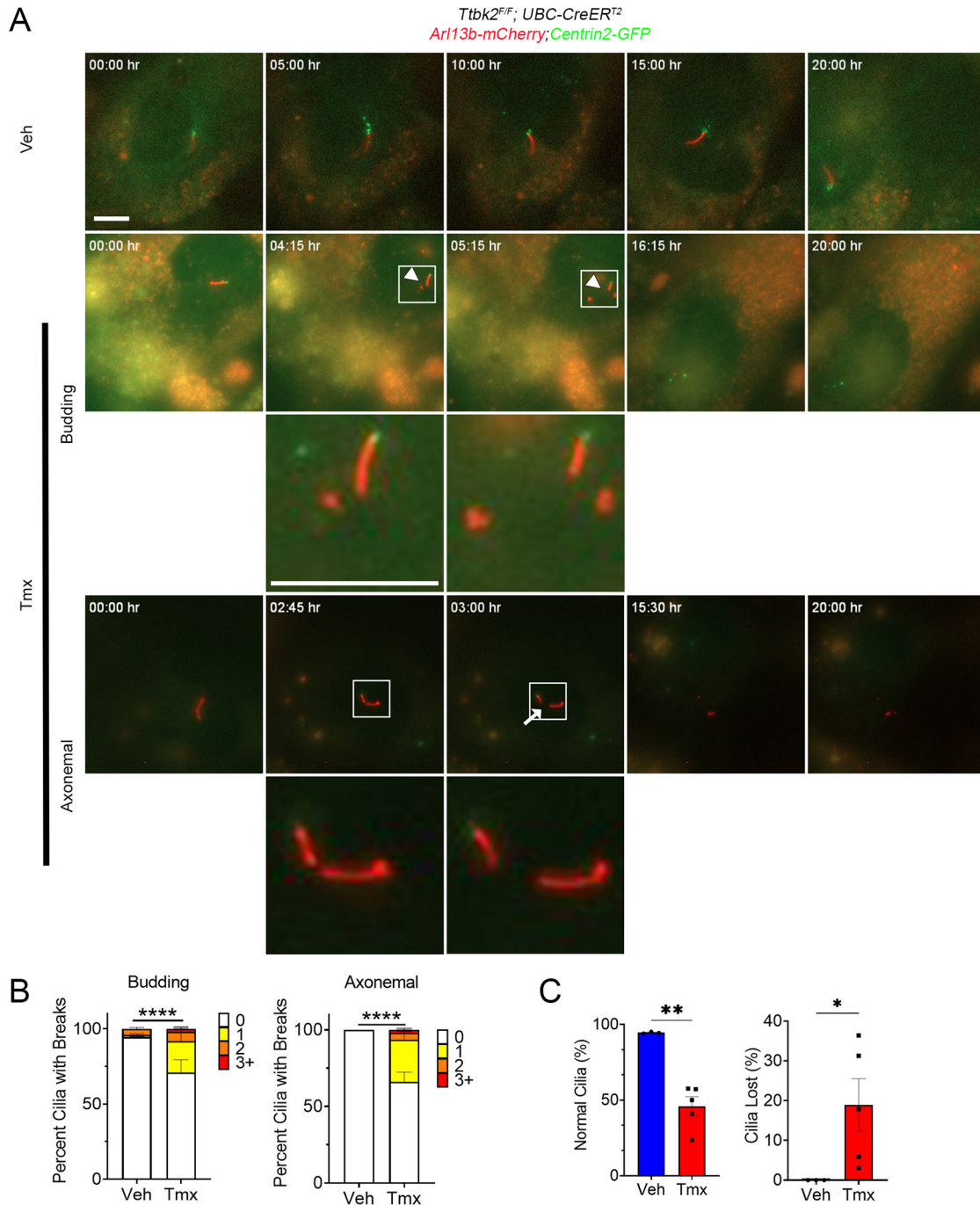
FIGURE 2: TTBK2 loss results in increased cilia fragmentation leading to cilia loss. (A) *Ttbk2cmut;ACCG* MEFs were serum-starved for 15 h before being treated with Veh or Tmx. Live imaging was then performed from 30 to 50 h after induction. Arrowheads show examples of cilia breakages at the ciliary tip resembling vesicles, termed "budding." Arrows show examples of cilia breakages along the axoneme resulting in large fragments of the cilia being removed, termed "axonemal." Insets are boxed, and magnifications are below their corresponding images. Time of video denotes hours:minutes into recording. Scale bars: 10 μm. (B) *Ttbk2cmut;ACCG* MEFs were treated with Veh and Tmx in three and five independent experiments, respectively. Each experiment had >16 observable cilia. Veh, $n = 110$; Tmx, $n = 132$. The graph depicts the mean percentage of cilia ± SEM observed having one, two, or ≥ three budding events or axonemal breaks. Statistical comparison was performed by a χ^2 test, ****$p < 0.0001$. (C) The graph depicts the percentage of cilia ± SEM observed not having any breaks (i.e. normal cilia). Each dot represents an experiment with >10 observable cilia. Statistical comparison was performed by an unpaired Student's t test, **$p < 0.01$. The graph depicts the percentage of cilia observed being lost by the end of the experiment. Each dot represents an experiment with an initial amount of cilia >10. Statistical comparison was performed by an unpaired nonparametric Student's t test, *$p < 0.05$.

FIGURE 3: Axonemal polyglutamylation is reduced upon *Ttbk2* deletion. (A) Representative images of *Ttbk2^cmut^* MEFs treated with Veh or Tmx for 0 and 72 h a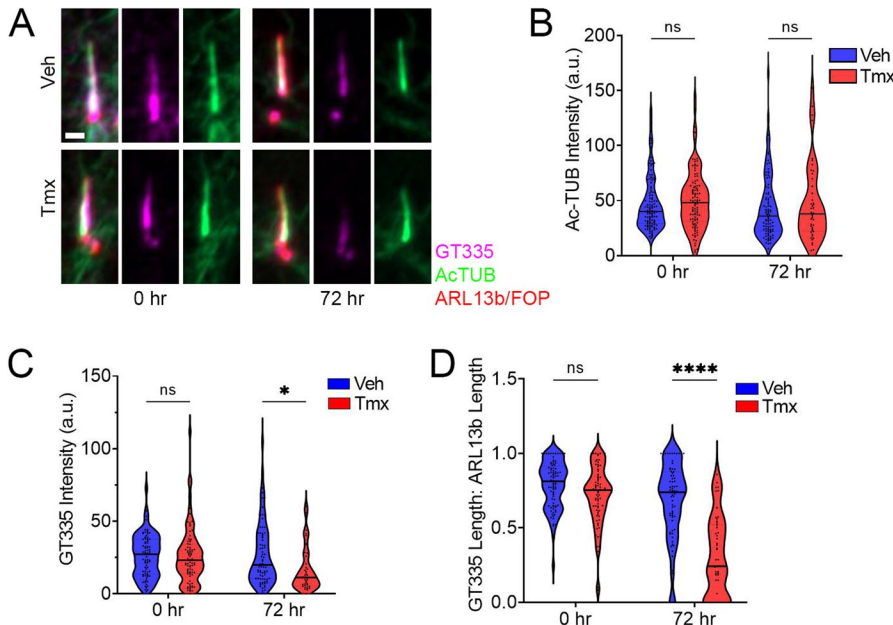nd stained for AcTUB (green), GT335 (magenta) to label polyglutamylated tubulin, and ARL13B and FOP (red) to label cilia and centrosomes, respectively. Scale bar: 1 μm. (B) The graph depicts the violin plot of the AcTUB intensity. Each dot represents a single measurement. Results are pooled from three independent experiments. Veh 0 h, $n = 114$; Veh 72 h, $n = 94$; Tmx 0 h, $n = 104$; Tmx 72 h, $n = 44$. Statistical comparison was performed by two-way ANOVA with Tukey's multiple comparisons test, ns denotes not significant. (C) The graph depicts the violin plot of GT335 intensity along the axoneme marked by ARL13B. Each dot represents a single measurement. Results are pooled from three independent experiments. Veh 0 h, $n = 79$; Veh 72 h, $n = 76$; Tmx 0 h, $n = 83$; Tmx 72 h, $n = 38$. Statistical comparison was performed by two-way ANOVA with Tukey's multiple comparisons test, ns denotes not significant, *$p < 0.05$. (D) The graph depicts the violin plot of the ratio of GT335 length to ARL13b length. Each dot represents a single measurement. Results are pooled from three independent experiments. Veh 0 h, $n = 81$; Veh 72 h, $n = 75$; Tmx 0 h, $n = 76$; Tmx 72 h, $n = 50$. Statistical comparison was performed by two-way ANOVA with Tukey's multiple comparisons test, ns denotes not significant, ****$p < 0.0001$.

cesses specifically at the cilium rather than throughout the entire cell. Loss of TTBK2 causes dysregulation of actin-related processes at the cilium immediately leading to cilia fragmentation.

Loss of TTBK2 results in changes to the centriolar satellites and deregulation of autophagy

Since perturbing the actin dynamics in *Ttbk2^cmut^* cells had only a transient stabilizing effect on cilia, this suggests that TTBK2 regulates other parallel processes that stabilize cilia. Inhibition of myosin VI partially attenuated cilia loss (Figure 4B). In addition to its role in the budding of ectosomes from the tips of cilia (Nager *et al.*, 2017), myosin VI is also linked to ciliogenesis through regulation of centriolar satellites (Magistrati *et al.*, 2021). We previously undertook biotin proximity labeling (BioID) with TTBK2 to identify proteins in the TTBK2 ciliogenesis pathway (Loukil *et al.*, 2021). In these studies, we found that of pericentriolar material and centriolar satellite-associated proteins as well as actin regulators were significantly enriched among the TTBK2-proximate hits (Loukil *et al.*, 2021) (Supplemental Table S1). We therefore examined the localization of myosin VI and the centriolar satellites in *Ttbk2^cmut^* MEFs treated with Tmx. Coimmunoprecipitation of TTBK2-V5 and a long and short isoform of myosin VI-GFP revealed that TTBK2 interacts with both isoforms (Wollscheid *et al.*, 2016) of myosin VI (Figure 5A). Consistent with our findings that inhibition of myosin VI can delay the loss of cilia in the absence of TTBK2, we found a significant accumulation of myosin VI at the basal body in *Ttbk2^cmut^* MEFs (Figure 5B).

but are not absent as at 72 h (Figure 1, B and C). In control cells, treatment with the drugs had no impact on the frequency of cilia, with the exception of the myosin VI inhibitor TIP, which modestly reduced cilia frequency (Figure 4, B and C). We also observed an increase in ciliary length in control cells treated with CytoD and TBSA, consistent with the known roles of actin polymerization and HDAC6 in limiting cilia length and promoting disassembly (Pugacheva *et al.*, 2007; Kim *et al.*, 2010; Ran *et al.*, 2015; Kohli *et al.*, 2017) (Figure 4D).

In Tmx-treated *Ttbk2^cmut^* cells, cotreatment with CytoD or the myosin VI inhibitor TIP resulted in increased cilia frequency at 48 h relative to treatment with DMSO, whereas the other inhibitors tested had no effect (Figure 4, B and C). This finding is consistent with the general role of actin polymerization in suppressing cilium assembly and promoting ciliary disassembly through budding and/or breakage (Nager *et al.*, 2017). These drugs had no effect on recombination, as TTBK2 levels decreased following treatment Tmx, similar to untreated cells (Supplemental Figure S3A). However, despite a higher frequency of cilia at 48 h post-Tmx treatment, by 72 h, cilia were lost regardless of inhibition of these actin regulators (Figure 4E). Additionally, whole-cell F-actin to G-actin levels were unchanged in Tmx-treated MEFs compared with Veh-treated MEFs. These data suggest that TTBK2 regulates actin-related pro-

Based on our findings for myosin VI, and our BioID data linking TTBK2 to the centriolar satellites, we hypothesized that dysfunction of the satellites might contribute to the cilium stability defects we observe in *Ttbk2^cmut^* MEFs treated with Tmx. Centriolar satellites play complex roles in cilium assembly. PCM1 is required for cilia assembly (Odabasi *et al.*, 2019), while other proteins such as OFD1 must be degraded at the satellites to promote cilia formation (Tang *et al.*, 2013). We therefore assessed the composition of the centriolar satellites and the localization of key satellite proteins, including PCM1, OFD1, and CEP290 in the *Ttbk2^cmut^* cells ± Tmx. PCM1 is the main component of the centriolar satellites and serves to scaffold, assemble, and maintain the satellites (Hori and Toda, 2017). We found that the intensity of PCM1 was dramatically decreased by 72 h post-Tmx treatment (Figure 5B), suggesting that TTBK2 might be important for the integrity of the satellites.

To determine if TTBK2 regulates other centriolar satellite components, we also assessed OFD1 and CEP290. OFD1 and CEP290, which both reside at the mother centriole in addition to the satellites, decline in intensity specifically at the satellites as serum starvation continues in control cells. However, both proteins remained elevated in *Ttbk2^cmut^* cells 72 h following treatment with Tmx (Figure 5, D and E). Total levels of the centriolar satellites did not change
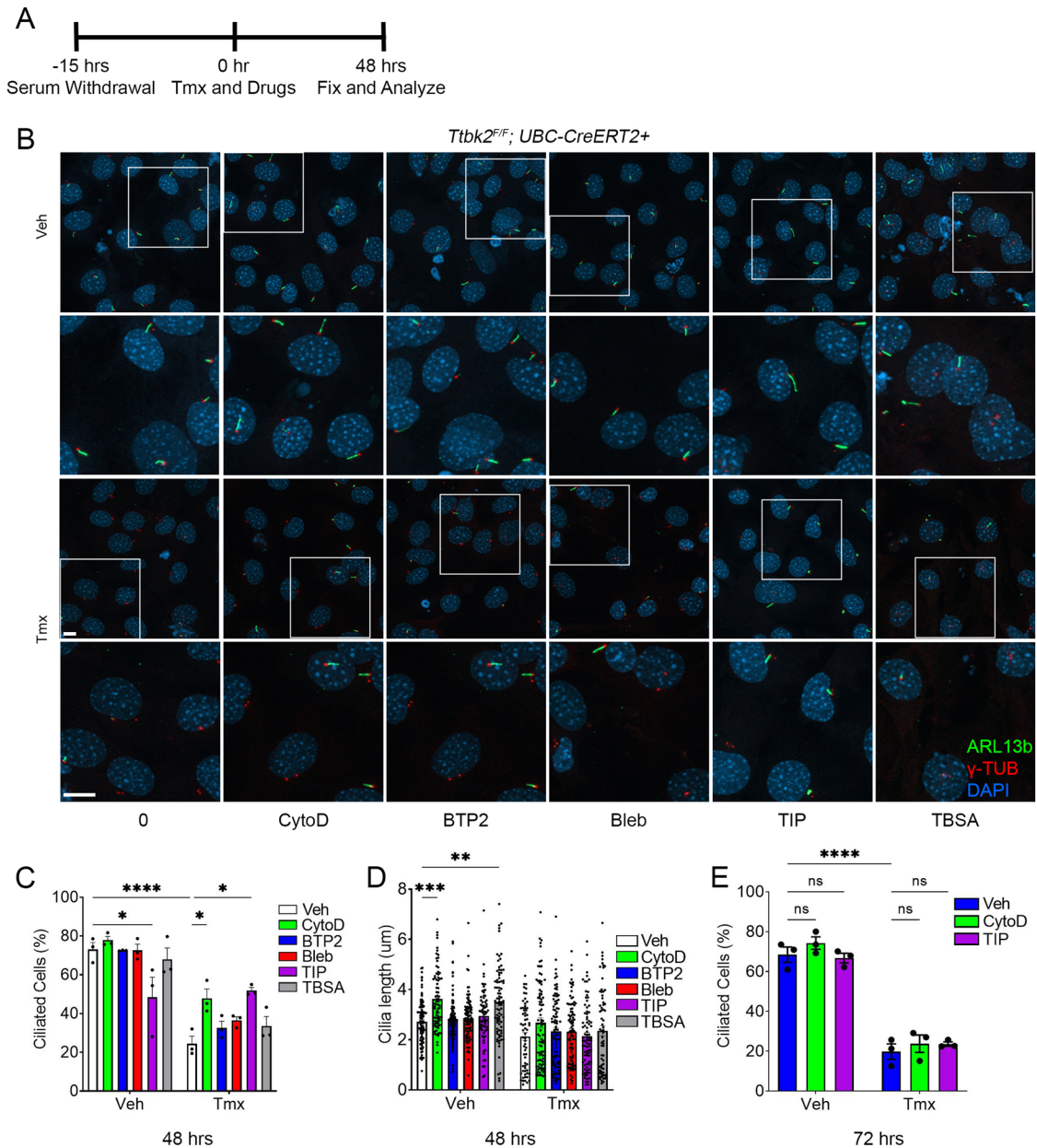
FIGURE 4: CytoD and TIP partially attenuate cilia loss due to TTBK2 deletion. (A) Schematic of experimental design. *Ttbk2^cmut* MEFs were serum-starved for 15 h before being treated with Veh or Tmx simultaneously with DMSO, CytoD (200 nM), Bleb (50μ M), BTP2 (1 μM), TIP (25 μM), or TBSA (2 μM) for 48 h. (B) Representative images of *Ttbk2^cmut* MEFs after being treated with Veh or Tmx with the indicated drugs for 48 h and stained for ARL13b (green), γ-tubulin (red), and DAPI (blue). Insets are boxed, and magnifications are below their corresponding images. Scale bars: 10 μm. (C) The graph depicts the mean percentage of ciliated cells ± SEM at 48 h. Each dot represents an experiment with >60 cells. Statistical comparison was performed by two-way ANOVA with Tukey's multiple comparisons test, *$p < 0.05$, ****$p < 0.0001$. (D) The graph depicts mean length of cilia ± SEM, measured at 48 h. Results are pooled from three independent experiments. Each dot represents a cilium ($n > 60$). Statistical comparison was performed by two-way ANOVA with Tukey's multiple comparisons test, **$p < 0.01$, ***$p < 0.001$. (E) The graph depicts the mean percentage of ciliated cells ± SEM at 72 h. Each dot represents an experiment with >60 cells. Statistical comparison was performed by two-way ANOVA with Tukey's multiple comparisons test, ns denotes not significant, ****$p < 0.0001$.

over time in Veh- and Tmx-treated *Ttbk2^cmut* cells (Supplemental Figure S4A). Similar defects in centriolar satellite composition are also seen in *Ttbk2^null/null* cells, namely, a decrease in PCM1 and an increase in OFD1 and CEP290 relative to WT cells (Supplemental Figure S4, B–D). In contrast, PCNT, a pericentriolar material protein, was not changed by loss of TTBK2, suggesting that these defects are limited to proteins found at the centriolar satellites (Figure 5F).

Mutation of a conserved aspartic acid to alanine in TTBK2's catalytic domain blocks its kinase activity (Bouskila *et al.*, 2011). While this kinase-dead TTBK2 correctly localizes to the mother centriole, it cannot rescue cilium assembly in *Ttbk2^null/null* cells (Goetz *et al.*, 2012), demonstrating that TTBK2 kinase activity is required for its role in cilium assembly. To determine if TTBK2 simply acts as a scaffold for centriolar satellites at the cilium or if its kinase activity is
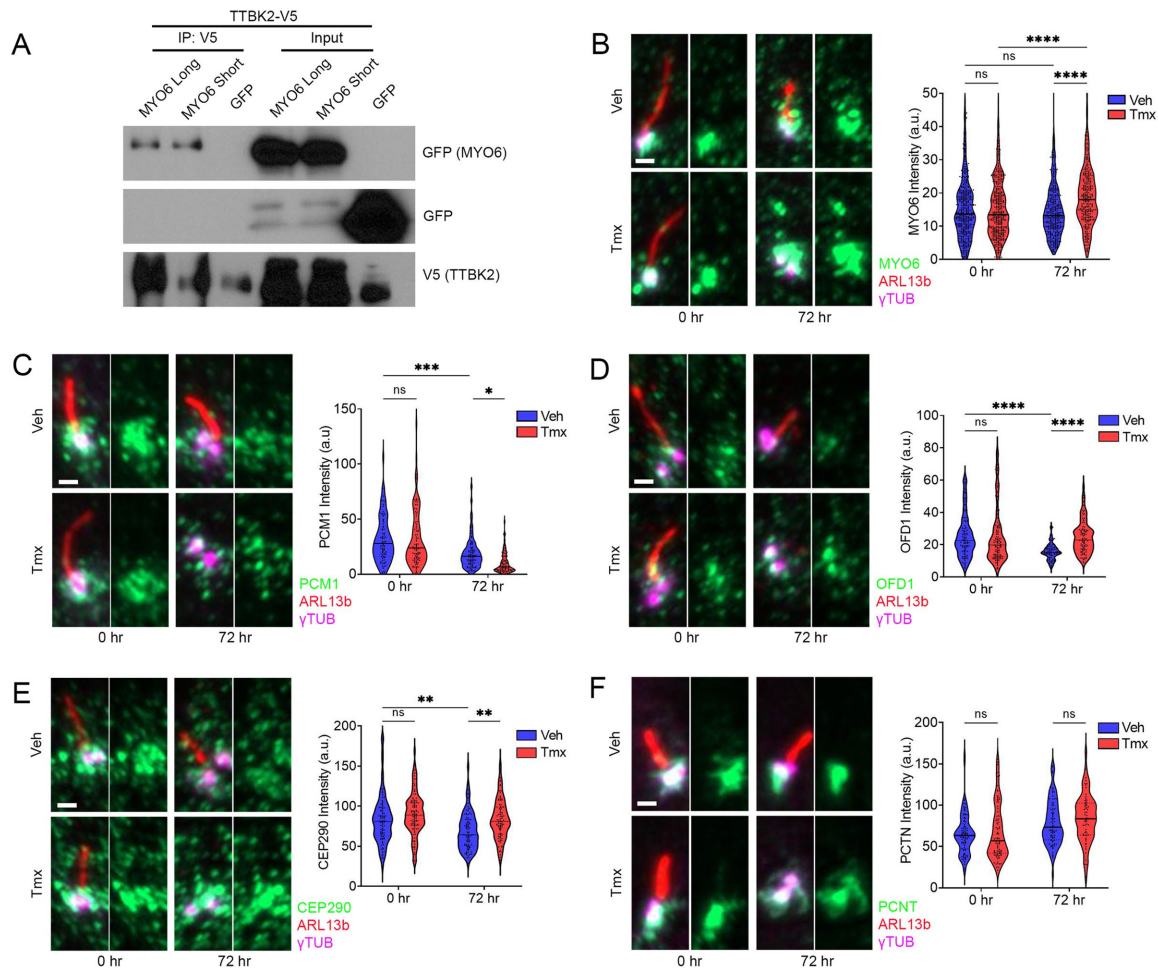
FIGURE 5: TTBK2 regulates the composition of the centriolar satellites. (A) Coimmunoprecipitation of HEK293T cells transfected with TTBK2-V5 and MYO6-GFP long, MYO6-GFP short, and GFP. Lysates were pulled down using V5 trap beads and blotted for GFP and V5. (B) Representative images of *Ttbk2cmut* MEFs treated with Veh or Tmx for 0 and 72 h and stained for MYO6 (green), ARL13b (red), and γ-tubulin (magenta). Scale bar: 1 μm. The graph depicts the mean intensity of MYO6 1μm around basal bodies. Results are pooled from three independent experiments. Each dot represents a single measurement from a basal body ($n > 275$). Statistical comparison was performed by two-way ANOVA with Tukey's multiple comparisons test, ns denotes not significant, *$p < 0.05$. (C) Representative images of *Ttbk2cmut* MEFs treated with Veh or Tmx for 0 and 72 h and stained for PCM1 (green), ARL13b (red), and γ-tubulin (magenta). Scale bar: 1 μm. The graph depicts the mean intensity of PCM1 1μm around basal bodies. Results are pooled from three independent experiments. Each dot represents a single measurement from a basal body ($n > 75$). Statistical comparison was performed by two-way ANOVA with Tukey's multiple comparisons test, ns denotes not significant, *$p < 0.05$. (D) Representative images of *Ttbk2cmut* MEFs treated with Veh or Tmx for 0 and 72 h and stained for OFD1 (green), ARL13b (red), and γ-tubulin (magenta). Scale bar: 1 μm. The graph depicts the mean intensity of OFD1 1μm around basal bodies. Results are pooled from three independent experiments. Each dot represents a single measurement from a basal body ($n > 75$). Statistical comparison was performed by two-way ANOVA with Tukey's multiple comparisons test, ns denotes not significant, ****$p < 0.0001$. (E) Representative images of *Ttbk2cmut* MEFs treated with Veh or Tmx for 0 and 72 h and stained for CEP290 (green), ARL13b (red), and γ-tubulin (magenta). Scale bar: 1 μm. The graph depicts the mean intensity of CEP290 1 μm around basal bodies. Results are pooled from three independent experiments. Each dot represents a single measurement from a basal body ($n > 75$). Statistical comparison was performed by two-way ANOVA with Tukey's multiple comparisons test, ns denotes not significant, **$p < 0.01$. (F) Representative images of *Ttbk2cmut* MEFs treated with Veh or Tmx for 0 and 72 h and stained for PCTN (green), ARL13b (red), and γ-tubulin (magenta). Scale bar: 1 μm. The graph depicts the mean intensity of PCTN at the basal bodies. Results are pooled from three independent experiments. Each dot represents a single measurement from a basal body ($n > 63$). Statistical comparison was performed by two-way ANOVA with Tukey's multiple comparisons test, ns denotes not significant.

required to regulate their composition, we stably expressed a kinase-dead TTBK2 or a WT TTBK2 in our *Ttbk2cmut* cells. Tmx-treated *Ttbk2cmut* cells stably expressing a kinase-dead TTBK2-GFP were unable to rescue PCM1 localization to the basal body, whereas *Ttbk2cmut* cells stably expressing WT TTBK2-GFP had restored PCM1 levels at centriolar satellites (Supplemental Figure S5A). Thus TTBK2 regulates the composition of the centriolar satellites after cilium assembly through its kinase activity.
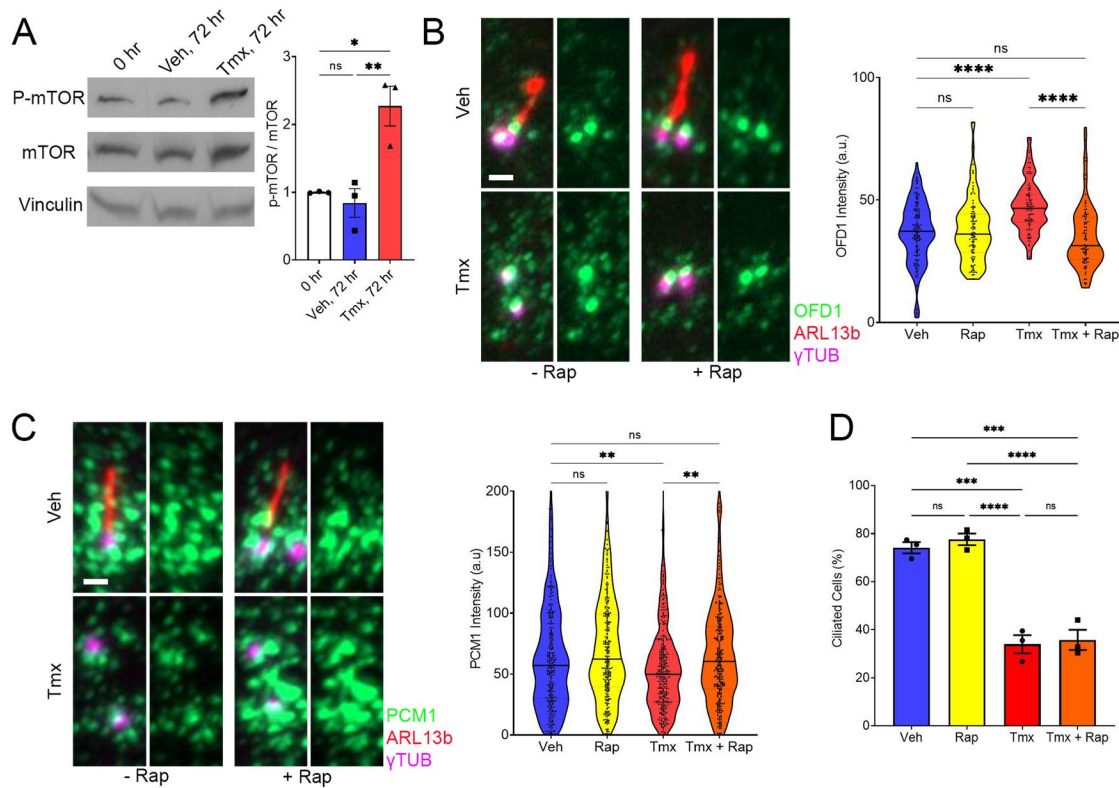
FIGURE 6: TTBK2 regulates the centriolar satellites through autophagy. (A) Western blot of P-mTOR, mTOR, and Vinculin from total lysates of *Ttbk2^cmut^* MEFs pretreated and treated with Veh or Tmx for 72 h. The graph depicts densitometric analysis of p-mTOR and mTOR levels of *Ttbk2^cmut^* MEFs treated with Veh or Tmx for 72 h normalized to pretreatment. Statistical comparison was performed by one-way ANOVA with Tukey's multiple comparisons test, ns denotes not significant, $*p < 0.05$, $**p < 0.01$. (B) Representative images of *Ttbk2^cmut^* MEFs treated with Veh, Rap, Tmx, or Tmx+Rap for 72 h and stained for OFD1 (green), ARL13b (red), and γ-tubulin (magenta). Scale bar: 1 µm. The graph depicts the mean intensity of OFD1 1 µm around basal bodies. Results are pooled from three independent experiments. Each dot represents a single measurement from a basal body ($n > 85$). Statistical comparison was performed by one-way ANOVA with Tukey's multiple comparisons test, ns denotes not significant, $****p < 0.0001$. (C) Representative images of *Ttbk2^cmut^* MEFs treated with Veh, Rap, Tmx, or Tmx+Rap for 72 h and stained for PCM1 (green), ARL13b (red), and γ-tubulin (magenta). Scale bar: 1 µm. The graph depicts the mean intensity of PCM1 1µm around basal bodies. Results are pooled from three independent experiments. Each dot represents a single measurement from a basal body ($n > 260$). Statistical comparison was performed by one-way ANOVA with Tukey's multiple comparisons test, ns denotes not significant, $**p < 0.01$. (D) The graph depicts the mean percentage of ciliated cells ± SEM. Each dot represents an experiment with >50 cells. Statistical comparison was performed by one-way ANOVA with Tukey's multiple comparisons test, ns denotes not significant, $***p < 0.001$, $****p < 0.0001$.

OFD1 is normally degraded at the centriolar satellites via autophagy to promote cilium assembly. In autophagy-deficient cells, OFD1 is retained at the satellites, inhibiting ciliogenesis (Tang *et al.*, 2013). The accumulation of OFD1 at the centriolar satellites in *Ttbk2^cmut^* cells suggested a deregulation of autophagy. Mammalian target of rapamycin (mTOR) regulates a number of cellular processes including cell growth, survival, metabolism, stress responses, and autophagy (Watanabe *et al.*, 2011). In nutrient-rich conditions, mTOR is phosphorylated at S2448 and inhibits autophagy (Melick and Jewell, 2020). Relative to the 0 time point, at 72 h, the ratio of phospho-mTOR to mTOR levels remained relatively unchanged in Veh-treated *Ttbk2^cmut^* cells, whereas Tmx-treated *Ttbk2^cmut^* cells had a higher phospho-mTOR to mTOR ratio (Figure 6A). This further supports a disruption in autophagy upon deletion TTBK2, due at least in part to mTOR activation.

Rapamycin promotes autophagy by interfering with mTOR's ability to bind to its effectors (Watanabe *et al.*, 2011) thereby inhibiting its activity. To test whether the centriolar satellite defects we observed in *Ttbk2^cmut^* cells are due to mTOR activation leading to reduced autophagy, we treated *Ttbk2^cmut^* cells with rapamycin and assessed whether we could rescue the cilia loss or other defects caused by TTBK2 deletion. Rapamycin did not change OFD1 levels in control cells but reduced OFD1 levels in Tmx-treated cells comparable with control cells (Figure 6B). Surprisingly, rapamycin also rescued PCM1 loss at the satellites in Tmx-treated cells (Figure 6C). However, despite restoring PCM1 and degrading OFD1 at the satellites, rapamycin was unable to restore cilia in Tmx-treated *Ttbk2^cmut^* cells (Figure 6D). Thus our data suggest that while TTBK2 regulates the centriolar satellite composition through autophagy, these defects do not fully drive the loss of cilia that occurs in the absence of TTBK2.

TTBK2 is required for pools of IFT proteins at the basal body that are essential to maintain the ciliary axoneme

Thus far, our data suggest that loss of TTBK2 destabilizes the cilium through the effects of both perturbed actin dynamics and dysregulation of the centriolar satellites. While the centriolar satellite
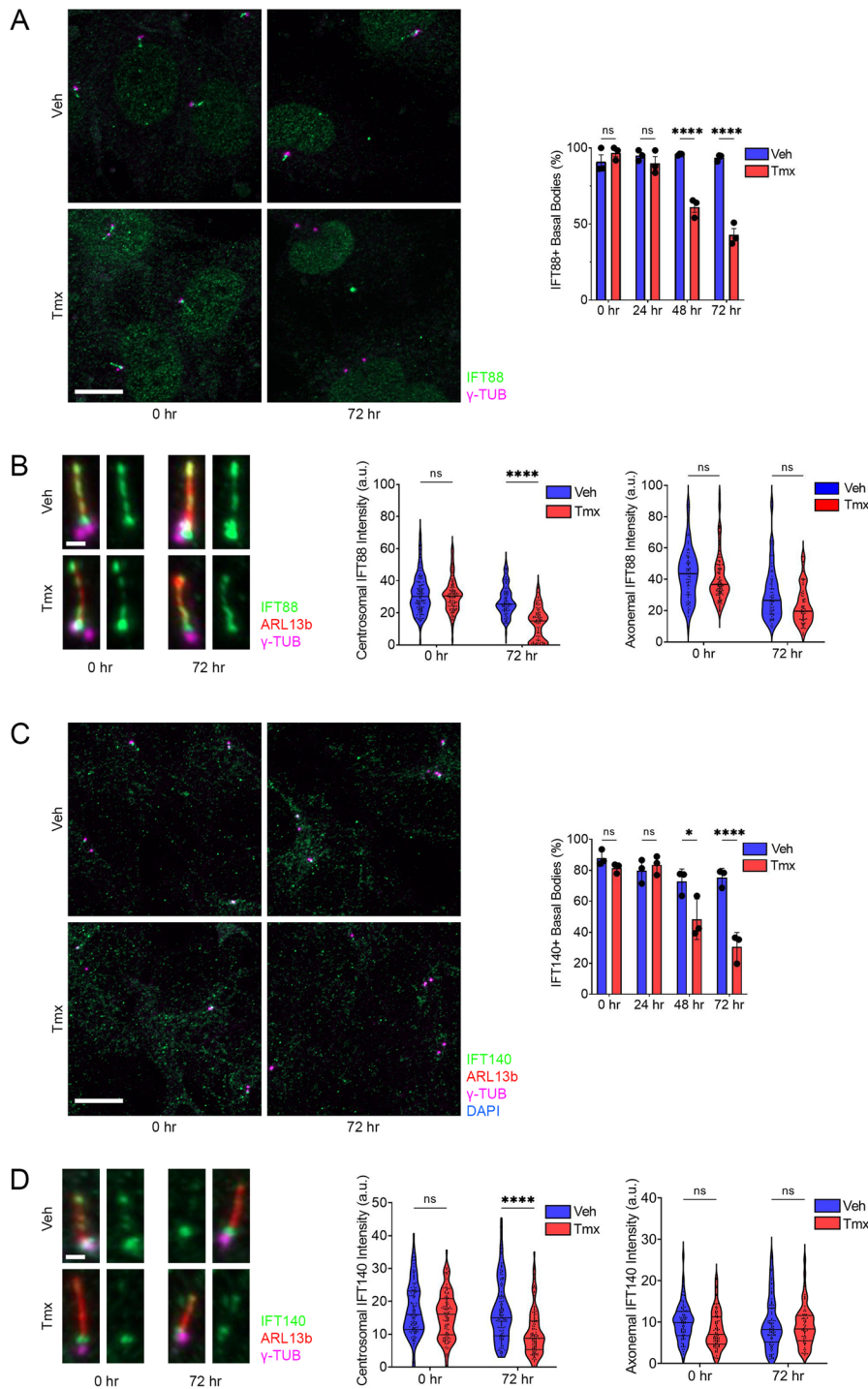
composition is disrupted due to *Ttbk2* deletion, restoration of PCM1 and OFD1 to levels comparable with control cells with rapamycin was not sufficient to rescue the cilia loss phenotype (Figure 6D). Other centrosome-associated proteins such as PCTN and the cilia disassembly proteins remain unchanged in the Tmx-treated *Ttbk2^cmut* cells (Figure 5E and Supplemental Figure S2). However, the axoneme exhibited dramatic changes such as increased cilia fragmentation (Figure 2, A–C) and reduced axonemal polyglutamylation (Figure 3, A–C). This suggests that loss of axonemal integrity may drive cilia loss in Tmx-treated *Ttbk2^cmut* cells, and we further reasoned that this loss of axonemal integrity may be due to disrupted trafficking by IFT proteins (Nakayama and Katoh, 2018; Pigino, 2021). Our previous work demonstrated that TTBK2 is required for the recruitment of IFT proteins to the mother centrioles prior to the assembly of the ciliary axoneme (Goetz *et al.*, 2012).

We therefore examined the localization of the IFTB component IFT88 and the IFTA component IFT140 to both the basal body pool and the ciliary axoneme in *Ttbk2^cmut* cells ± Tmx over the 72-h time course. We found that for both IFT88 and IFT140, the percentage of cells with IFT protein at the basal body

FIGURE 7: TTBK2 maintains the basal body pools of IFT. (A) Representative images of *Ttbk2^cmut* MEFs treated with Veh or Tmx for 0 and 72 h and stained for IFT88 (green), ARL13b (red), γ-tubulin (magenta), and DAPI (blue). Scale bar: 10 μm. The graph depicts the mean percentage of basal bodies with IFT88 ± SEM. Each dot represents an experiment with >50 basal bodies. Statistical comparison was performed by two-way ANOVA with Tukey's multiple comparisons test, $****p < 0.0001$. (B) Representative images of *Ttbk2^cmut* MEFs treated with Veh or Tmx for 0 and 72 h and stained for IFT88 (green), ARL13b (red), and γ-tubulin (magenta). Scale bar: 1 μm. The graph depicts the mean intensity of IFT88 at basal bodies. Results are pooled from three independent experiments. Each dot represents a single measurement from a basal body ($n > 75$). Statistical comparison was performed by two-way ANOVA with Tukey's multiple comparisons test, ns denotes not significant, $****p < 0.0001$. The graph depicts the mean intensity of IFT88 along the axoneme. Results are pooled from three independent experiments. Each dot represents a single measurement from a basal body. Veh 0 h, $n = 76$; Veh 72 h, $n = 72$; Tmx 0 h, $n = 95$; Tmx 72 h, $n = 57$. Statistical comparison was performed by two-way ANOVA with Tukey's multiple comparisons test, ns denotes not significant. (C) Representative images of *Ttbk2^cmut* MEFs treated with Veh or Tmx for 0 and 72 h and stained for IFT140 (green), ARL13b (red), γ-tubulin (magenta), and DAPI (blue). The graph depicts the mean percentage of basal bodies with IFT88 ± SEM. Each dot represents an experiment with >50 basal bodies. Scale: 10 μm. Statistical comparison was performed by two-way ANOVA with Tukey's multiple comparisons test, $*p < 0.05$, $****p < 0.0001$. (D) Representative images of *Ttbk2^cmut* MEFs treated with Veh or Tmx for 0 and 72 h and stained for IFT140 (green), ARL13b (red), and γ-tubulin (magenta). Scale bar: 1 μm. The graph depicts the mean intensity of IFT140 at basal bodies. Results are pooled from three independent experiments. Each dot represents a single measurement from a basal body ($n > 75$). Statistical comparison was performed by two-way ANOVA with Tukey's multiple comparisons test, ns denotes not significant, $****p < 0.0001$. The graph depicts the mean intensity of IFT140 along the axoneme. Results are pooled from three independent experiments. Each dot represents a single measurement from a basal body. Veh 0 h, $n = 77$; Veh 84 h, $n = 72$; Tmx 0 h, $n = 89$; Tmx 72 h, $n = 61$. Statistical comparison was performed by two-way ANOVA with Tukey's multiple comparisons test, ns denotes not significant.
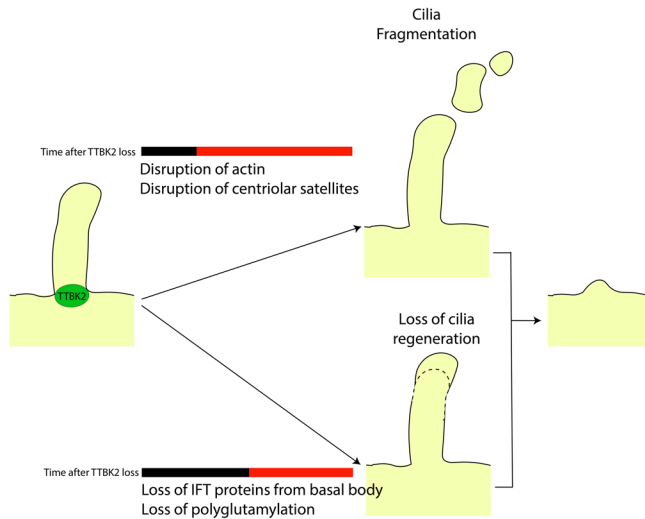
FIGURE 8: TTBK2 maintains primary cilia through multiple pathways. TTBK2 maintains primary cilia by regulating polyglutamylation of the axoneme, actin dynamics at the cilia, the composition of the centriolar satellites, and the retention of IFT proteins at the basal body. Loss of TTBK2 leads to cilia fragmentation events driven by loss of polyglutamylation, a disruption in ciliary actin dynamics, and a disruption of the centriolar satellite composition. In a separate pathway, IFT proteins are lost resulting in an inability for the primary cilia to recover.

declines within 48 h of Tmx treatment (Figure 7, A and C). This also corresponds with when cilia begin to disappear in the *Ttbk2cmut* cells treated with Tmx (Figure 1C). Analysis of fluorescence intensity revealed that at 72 h post-Tmx treatment, the *Ttbk2cmut* cells showed diminished levels of both IFT88 and IFT140 in the basal body pools. By contrast, the intensity of both IFT proteins within the remaining ciliary axonemes was not significantly affected (Figure 7, B and D). Additionally, stable expression of WT and the kinase-dead TTBK2-GFP revealed that TTBK2's kinase activity is also required for the maintenance of IFT proteins at the basal body as WT TTBK2-GFP was able to rescue IFT88 loss at the basal body in Tmx-treated *Ttbk2cmut* cells but the kinase-dead TTBK2-GFP was not (Supplemental Figure S5C). This suggests that the basal body pool of IFT proteins plays a critical role in maintaining the integrity of the ciliary axoneme, and that TTBK2 is required to maintain this pool following cilium assembly, in addition to recruiting IFT proteins during ciliogenesis.

Our findings suggest that TTBK2 regulates primary cilia stability through parallel pathways (Figure 8). TTBK2 prevents cilia fragmentation by controlling actin dynamics after ciliogenesis. It also regulates the composition of the centriolar satellites through its kinase activity and autophagy. Finally, in addition to being required for IFT recruitment during ciliogenesis, TTBK2 is required for the retention or replenishment of IFT pools at the basal body. These findings reveal multiple mechanisms by which the primary cilium is maintained after being assembled.

DISCUSSION

In this study, we use an inducible genetic system to assess the requirements for TTBK2 in maintaining cilia structure. Using these tools, we were able to perturb cilia after cells had undergone ciliogenesis through Tmx-induced deletion of *Ttbk2*. This has allowed us to assess the dynamic changes to primary cilia as TTBK2 is lost and uncover additional requirements for TTBK2 in regulating primary cilia.

Our previous work suggested that TTBK2 regulates primary cilia structure and stability; however, the precise mechanisms by which TTBK2 does this were unknown. Serum readdition following the induction of cilia results in cilia disassembly in cultured fibroblasts and correlates with TTBK2 loss or removal from the basal body (Goetz *et al.*, 2012). Cells with hypomorphic mutations in TTBK2 form unstable cilia (Bowie *et al.*, 2018) and deletion of TTBK2 in adult mice results in reduced cilia frequency in the adult brain as rapidly as 15 d following Tmx induction in *Ttbk2cmut* mice (Bowie and Goetz, 2020). In this study, we visualize how cilia loss occurs in the absence of TTBK2 through live imaging. While a low frequency of ciliary excision from the tip is proposed to be a mechanism for maintaining ciliary length (Ford *et al.*, 2018), both the proportion of cilia that form buds and the frequency of budding events per cilium increase when TTBK2 is depleted. Additionally, some cilia shed larger fragments of the axoneme upon TTBK2 loss, reminiscent of whole cilium shedding events that have been linked to cilia disassembly (Mirvis *et al.*, 2019). Ciliary excision and whole cilium shedding can be attenuated using actin inhibitors and HDAC6 inhibition, respectively (Nager *et al.*, 2017; Mirvis *et al.*, 2019). The similarities between these studies and our observations prompted us to assess whether TTBK2 maintains primary cilia by regulating actin dynamics and/or suppressing the cilia disassembly pathway. *Ttbk2* deletion does not alter the localization of the cilia disassembly proteins KIF2A, PLK1, or phospho-AURKA at the basal body, suggesting that TTBK2 does not principally regulate cilia maintenance by suppressing cilia disassembly proteins. Corroborating this finding, we also show that treatment of *Ttbk2cmut* cells with the HDAC6 inhibitor TBSA did not lead to rescue in cilia frequency at any point in our time-course.

We treated Tmx-treated *Ttbk2cmut* cells with other small molecule inhibitors previously shown to suppress primary cilia excision. Only CytoD and TIP partially rescued cilia loss. CytoD inhibits actin polymerization and TIP inhibits myosin VI, a motor protein that directs movement toward the minus end of actin filaments. Consistent with TIP transiently attenuating cilia loss resulting from TTBK2 deletion, myosin VI levels were increased at the centrioles in Tmx-treated *Ttbk2cmut* cells. It is possible that CytoD attenuates cilia loss through the same mechanism as TIP by preventing myosin VI-dependent trafficking of proteins to the cilium. Therefore TTBK2 may mediate primary cilia stability by regulating actin-based trafficking to the cilium.

There is additional evidence to suggest that TTBK2 interacts with actin-regulatory proteins to regulate primary cilia stability. In addition to its role in regulating cilium assembly, TTBK2 is also linked to cytoplasmic microtubule dynamics (Liao *et al.*, 2015; Watanabe *et al.*, 2015), and recent studies point to cross-talk between microtubules and actin filaments (Farina *et al.*, 2019; Inoue *et al.*, 2019). Recent work from our lab identified CSNK2A1 as a direct interactor of TTBK2 that negatively modulates TTBK2 function at the ciliary base (Loukil *et al.*, 2021). In CSNK2A knockout cells, cilia are unstable, undergoing frequent excision events, and actin and actin modulators are enriched at the ciliary tip, associated with those excision events (Loukil *et al.*, 2021). Our TTBK2 BioID screen also identified several actin regulators as TTBK2-proximate proteins (Loukil *et al.*, 2021). These data suggest that TTBK2 mediates cilia stability by limiting cilia fragmentation in part by regulating actin or actin-related processes.

In addition to its role in trafficking proteins along actin filaments, myosin VI reportedly regulates centriolar satellite composition (Magistrati *et al.*, 2021). Recent evidence also suggests that the centriolar satellite scaffold PCM1 is also involved in cilia maintenance (Aydin *et al.*, 2020). The centriolar satellites were accordingly disrupted as a function of *Ttbk2* deletion, with PCM1 being lost and OFD1 and CEP290 being abnormally retained or accumulating in

the absence of TTBK2. Previous studies showed that silencing or inhibiting myosin VI blocks cilia ectocytosis presumably through its actin-associated roles (Nager *et al.*, 2017), but since myosin VI also regulates the centriolar satellites, it is possible that the centriolar satellites also promote cilium stability by limiting cilia fragmentation events. TTBK2's kinase activity is required for ciliogenesis and the maintenance of PCM1 at the basal body, and TTBK2 coimmunoprecipitates with myosin VI, but whether TTBK2 directly phosphorylates PCM1 or myosin VI remains to be determined.

In addition to PCM1, TTBK2 also regulates the levels of OFD1 and CEP290 at the satellites and basal body. While TTBK2 maintains PCM1 levels, it appears to promote the degradation of OFD1 and CEP290 at the satellites. Prior work has shown that while OFD1 recruitment to the centriole is required for the maturation of the mother centriole and therefore the initiation of ciliogenesis (Singla *et al.*, 2010), its degradation by autophagy at the satellites is also required for cilium assembly (Tang *et al.*, 2013). Serum starvation induces autophagy (Seeley and Nachury, 2010), and autophagy promotes the degradation of OFD1 at the satellites (Tang *et al.*, 2013). Our data suggest that cells are continuing to undergo autophagy during serum withdrawal even after ciliogenesis is underway and reveal that TTBK2 is involved in this process since mTOR phosphorylation increases and OFD1 accumulates when TTBK2 is lost after cilium assembly. Rapamycin inhibits mTOR activity (Watanabe *et al.*, 2011) and promotes autophagy. Rapamycin-induced autophagy restores OFD1 to levels comparable with those of control cells, suggesting that the mTOR-mediated autophagy is linked to OFD1 degradation, and that TTBK2 inhibits mTOR activation.

PCM1 and OFD1 colocalize to centriolar satellites, and their interaction is well established (Lopes *et al.*, 2011; Tang *et al.*, 2013; Aydin *et al.*, 2020). PCM1 is proposed to mediate OFD1 degradation by facilitating its interaction with LC3 which targets OFD1 for degradation (Tang *et al.*, 2013). Interestingly, rapamycin-induced autophagy is also able to restore PCM1 levels around the basal body, suggesting that autophagy not only promotes the degradation of OFD1 but also maintains PCM1 levels at the satellites—perhaps even regulating the composition of the centriolar satellites as a whole. Our BioID screen also identified several autophagy-related proteins as proximate to TTBK2, suggesting that TTBK2 may interact with these proteins. Further molecular characterization of the links between TTBK2 and autophagy will be the subject of future studies by our lab.

Neither restoration of the centriolar satellites by inducing autophagy nor disrupting actin polymerization fully rescued the cilia loss that results from *Ttbk2* deletion, prompting us to assess IFT. IFT is required not only for cilium assembly but also to maintain cilia structure through continuous trafficking. Tmx-induced deletion of *Ift88* in the kidneys and in the brain leads to a loss of primary cilia in adult mice (Davenport *et al.*, 2007). Recent work suggests that IFT is recruited to the basal body by a diffusion-to-capture mechanism (Hibbard *et al.*, 2021), though how the basal body "captures" IFT remains unknown. Our work reveals that in addition to its role in IFT recruitment during cilium assembly, TTBK2 is also indispensable for IFT maintenance after cilium assembly. Our results suggest that TTBK2 is involved in modifying the basal body such that it continually replenishes IFT. In the absence of TTBK2, the basal body IFT pools therefore become depleted and ultimately disappear. The mother centriole's DAs are required for TTBK2 recruitment (Tanos *et al.*, 2013; Čajánek and Nigg, 2014). In addition, several recent studies have shown that TTBK2 phosphorylates some of these DA proteins including CEP83, CEP89, and CEP164 (Lo *et al.*, 2019; Bernatik *et al.*, 2020) modifications that may be required for the capture and retention of IFT proteins.

In sum, our study supports a model in which TTBK2 acts via multiple mechanisms to regulate cilium initiation and maintenance, underscoring the central role of this kinase in regulating primary cilia. We propose that TTBK2 regulates composition of the centrosome which contributes to building and maintaining stable primary cilia. Our data suggest that TTBK2 regulates the actin network near the basal body the centriolar satellites via autophagy. *Ttbk2* deletion causes dysregulation of actin-based trafficking and of centriolar satellites leading to loss of axonemal integrity and its fragmentation. In a separate pathway, TTBK2 regulates IFT recruitment and retention at the basal body, which in turn maintains the axonemal composition and length.

MATERIALS AND METHODS
Request a protocol through *Bio-protocol*.

Ethics statement
The use and care of mice as described in this study were approved by the Institutional Animal Care and Use Committee, Duke University (approval numbers A218-17-09 and A175-20-08). Euthanasia for the purpose of harvesting embryos was performed by cervical dislocation, and all animal studies were performed in compliance with internationally accepted standards.

Mouse strains
Mouse strains used in this study were *Ttbk2*^loxP/loxP^ (*Ttbk2*^f/f^) mice generated in a previous study (Bowie and Goetz, 2020), *UBC-Cre-ERT2* mice were acquired from Jackson Laboratory (#007001), and *Arl13b-mCherry;Centrin2-GFP* mice were kindly donated from K.V. Anderson (Bangs *et al.*, 2015).

Cell culture
Ttbk2F/F; UBC-CreERT2+ MEFs were derived from embryonic day (E) 10.5 mouse embryos and cultured in DMEM supplemented with 10% FBS and 1% penicillin/streptomycin (P/S) (cDMEM) at 5% CO_2 at 37°C. Unless indicated otherwise, cells were plated on gelatin-coated coverslips and serum-starved for 15 h in DMEM supplemented with 0.5% FBS and 1% P/S. Cells were then treated with ethanol (Veh) or 1 μm 4-hydroxytamoxifen (Tmx) for the indicated duration in serum-starved conditions.

Transient and sable transfection
MEFs were transfected using Lipofectamine 2000 (ThermoFisher 11668) in OptiMEM (Life Technologies 31985). For stable expression of TTBK2-GFP and the kinase-dead TTBK2-GFP, retroviruses were produced and used to infect MEFs according to standard protocols. MEFs were then put under 500 μg/ml G418 selection. Plasmids used were pFLAP-Dest-TTBK2 described previously (Goetz *et al.*, 2012). Myosin VI-GFP constructs were kindly provided by S. Polo (Magistrati *et al.*, 2021).

Drug and inhibitor treatment
Drugs were added to cells at the time of Tmx induction at the following concentrations: CytoD (Santa Cruz SC-201442; 200 nM in DMSO), blebbistatin (VWR S7099; 50 μm in DMSO), BTP2 (Abcam ab144413; 1 μm in DMSO), rapamycin (Cell Signaling 99045; 25 nM in DMSO), TBSA (Tocris 6270; 2 μm), and TIP (Sigma 137723) (25 μm).

Immunofluorescence
Cells were then fixed in 4% paraformaldehyde for 5 min and then ice-cold methanol for 5 min, washed 3× with phosphate-buffered saline (PBS) for 5 min each, and blocked with PBS + 5% goat serum

+ 1% BSA + 0.1% Triton X-100 (blocking buffer) for 30 min. Next, cells were incubated with primary antibodies diluted in blocking buffer overnight at 4°C, washed 3× with PBS for 5 min each, and incubated with secondary antibodies diluted in blocking buffer for 30 min at room temperature. Finally, cells were stained with DAPI in PBS for 5 min, washed two additional times with PBS for 5 min each, and mounted onto glass slides using Prolong Gold (Invitrogen P36930).

Antibodies

Primary antibodies used were mouse anti-ARL13b (NeuroMab 75-287), rabbit anti-ARL13b (Proteintech 17711-1-AP), rabbit anti-phospho-Aurora A (Cell Signaling 3079), rabbit anti-CEP290 (Proteintech 22490-1-AP), rabbit anti-GFP (Invitrogen A11122), rabbit anti-FOP (Proteintech 11343-1-AP), mouse anti-GFP (Proteintech 66002-1-Ig), rabbit anti-IFT88 (Proteintech-11744), rabbit anti-IFT140 (Proteintech 17460-1-AP), rabbit anti-KIF2A (Abcam ab37005), rabbit anti-OFD1 (kindly donated from JF Reiter), rabbit anti-mTOR (Cell Signaling 2971), rabbit anti-phospho-mTOR (Cell signaling 2983), rabbit anti-PCM1 (Proteintech 19856-1-AP), rabbit anti-PCNT (Biolegend 923701), mouse anti-PLK1 (Thermofisher 33-1700), rabbit anti-TTBK2 (Sigma HPA018113), and mouse anti-γ-tubulin (Sigma-Aldrich T6557).

Microscopy

Immunofluorescence images were taken using a Zeiss AxioObserver wide field microscope equipped with an Axiocam 506 mono camera and Apotome.2 optical sectioning with structured illumination. Z-stacks were taken at 0.5-μm intervals and maximum intensity projections were then created. Image processing and quantifications were performed using ImageJ. In brief, cilia frequency was quantified by counting the number of ARL13b+ cells versus DAPI+ cells. For intensity measurements, background was subtracted, and the mean intensity was recorded for a drawn region of interest. For centriolar satellite proteins, a 1 μm ROI was made around the basal body and the intensity was then measured. For measurements of proteins along the axoneme, a line was drawn along the axoneme with the exclusion of the basal body and the intensity was measured. For all other measurements, a free-form tool was used to select the ROI.

Western blotting

Ttbk2cmut MEFs were plated in a 10-cm plate and allowed to reach confluency before being serum-starved for 15 h. Cells were then given Veh or Tmx for 0 or 72 h and lysed in RIPA buffer (150 mM NaCl, 1% NP-40, 0.5% sodium deoxycholate, 0.1% SDS, 50 mM Tris, pH 8.0). Protein concentration was measured using a BCA assay and samples were boiled at 95°C for 5 min to denature proteins. Total lysates were separated by SDS–PAGE and transferred onto a PVDF membrane. The membrane was blocked with 5% milk in TBST for 1 h at RT, incubated with primary antibodies in blocking buffer overnight at 4C, and incubated with HRP–conjugated secondary antibodies for 1 h at RT. Membranes were developed with an ECL. Western blots were analyzed using densitometric analysis in FIJI.

F-actin/G-actin quantification

F-actin and G-actin were purified using the G-actin/F-actin In Vivo Assay Kit from Cytoskeleton (Cat No. BK037). Briefly, *Ttbk2cmut* MEFs were plated in a 6-well plate, serum-starved, and treated with Veh or Tmx. They were then lysed in a buffer that precipitated F-actin and ultracentrifuged at $100,000 \times g$ for 1 h at 37°C. Supernatants possessing G-actin were collected and the F-actin precipitate was solubilized. Both were then assessed by Western blot.

Time-lapse imaging

Ttbk2cmut;ACCG MEFs were seeded in an 8-well μ-Slide (IBIDI 80826), serum-starved, and treated with ethanol or Tmx. The cells were then imaged at 15-min intervals from 30 to 50 h post-Tmx induction in an incubation chamber maintained with 5% CO_2 at 37°C by a Pecon CO2 Module S and TempModule S. The recorded cilia were then manually analyzed frame by frame for abnormalities and loss using Zen 2.0. Abnormalities included but were not limited to cilia fragmentation events referred to as "budding" where a vesiclelike fragment of the cilia was removed from the tip of the cilia and "axonemal" where a larger fragment of the cilia (those bigger than a vesicle) was removed from the main cilia still attached to Centrin2-GFP.

Quantification and statistics

Data are reported as arithmetic means ± SEM. Statistical analysis was done with GraphPad Prism 8. Most experiments were analyzed using a two-way ANOVA and a Tukey post-hoc test.

REFERENCES

Aydin ÖZ, Taflan SO, Gurkaslar C, Firat-Karalar EN (2020). Acute inhibition of centriolar satellite function and positioning reveals their functions at the primary cilium. PLoS Biol 18, e3000679.

Bangs FK, Schrode N, Hadjantonakis A-K, Anderson KV (2015). Lineage specificity of primary cilia in the mouse embryo. Nat Cell Biol 17, 113–122.

Bernatik O, Pejskova P, Vyslouzil D, Hanakova K, Zdrahal Z, Cajanek L (2020). Phosphorylation of multiple proteins involved in ciliogenesis by Tau Tubulin kinase 2. Mol Biol Cell, mbcE19060334.

Bouskila M, Esoof N, Gay L, Fang EH, Deak M, Begley MJ, Cantley LC, Prescott A, Storey KG, Alessi DR (2011). TTBK2 kinase substrate specificity and the impact of spinocerebellar-ataxia-causing mutations on expression, activity, localization and development. Biochem J 437, 157–167.

Bowie E, Goetz SC (2020). TTBK2 and primary cilia are essential for the connectivity and survival of cerebellar Purkinje neurons. Elife 9, 1–24.

Bowie E, Norris R, Anderson KV, Goetz SC (2018). Spinocerebellar ataxia type 11-associated alleles of Ttbk2 dominantly interfere with ciliogenesis and cilium stability. PLoS Genet 14, e1007844.

Bowler M, Kong D, Sun S, Nanjundappa R, Evans L, Farmer V, Holland A, Mahjoub MR, Sui H, Loncarek J (2019). High-resolution characterization of centriole distal appendage morphology and dynamics by correlative STORM and electron microscopy. Nat Commun 10, 993.

Čajánek L, Nigg EA (2014). Cep164 triggers ciliogenesis by recruiting Tau tubulin kinase 2 to the mother centriole. Proc Natl Acad Sci USA 111, E2841–E2850.

Craft JM, Harris JA, Hyman S, Kner P, Lechtreck KF (2015). Tubulin transport by IFT is upregulated during ciliary growth by a cilium-autonomous mechanism. J Cell Biol 208, 223–237.

Davenport JR, Watts AJ, Roper VC, Croyle MJ, van Groen T, Wyss JM, Nagy TR, Kesterson RA, Yoder BK (2007). Disruption of intraflagellar transport in adult mice leads to obesity and slow-onset cystic kidney disease. Curr Biol 17, 1586–1594.

Farina F, Ramkumar N, Brown L, Eweis DS, Anstatt J, Waring T, Bithell J, Scita G, Thery M, Blanchoin L, *et al.* (2019). Local actin nucleation tunes centrosomal microtubule nucleation during passage through mitosis. EMBO J 38, e99843.

Ford MJ, Yeyati PL, Mali GR, Keighren MA, Waddell SH, Mjoseng HK, Douglas AT, Hall EA, Sakaue-Sawano A, Miyawaki A, *et al.* (2018). A cell/cilia cycle biosensor for single-cell kinetics reveals persistence of cilia after G1/S transition is a general property in cells and mice. Dev Cell 47, 509–523.e5.

Goetz SC, Anderson KV (2010). The primary cilium: a signalling centre during vertebrate development. Nat Rev Genet 11, 331–344.

Goetz SC, Liem KF Jr, Anderson KV (2012). The spinocerebellar ataxia-associated gene Tau tubulin kinase 2 controls the initiation of ciliogenesis. Cell 151, 847–858.

He K, Ling K, Hu J (2020). The emerging role of tubulin posttranslational modifications in cilia and ciliopathies. Biophys Rep 6, 89–104.

He M, Subramanian R, Bangs F, Omelchenko T, Liem KF Jr, Kapoor TM, Anderson KV (2014). The kinesin-4 protein Kif7 regulates mammalian Hedgehog signalling by organizing the cilium tip compartment. Nat Cell Biol 16, 663–672.

Hibbard JVK, Vazquez N, Satija R, Wallingford JB (2021). Protein turnover dynamics suggest a diffusion-to-capture mechanism for peri-basal body recruitment and retention of intraflagellar transport proteins. Mol Biol Cell 32, 1171–1180.

Higginbotham H, Bielas S, Tanaka T, Gleeson JG (2004). Transgenic mouse line with green-fluorescent protein-labeled Centrin 2 allows visualization of the centrosome in living cells. Transgenic Res 13, 155–164.

Hilgendorf KI, Johnson CT, Jackson PK (2016). The primary cilium as a cellular receiver: organizing ciliary GPCR signaling. Curr Opin Cell Biol 39, 84–92.

Hori A, Toda T (2017). Regulation of centriolar satellite integrity and its physiology. Cell Mol Life Sci 74, 213–229.

Inoue D, Obino D, Pineau J, Farina F, Gaillard J, Guerin C, Blanchoin L, Lennon-Duménil A-M, Théry M (2019). Actin filaments regulate microtubule growth at the centrosome. EMBO J 38, 1–15.

Kim J, Lee JE, Heynen-Genel S, Suyama E, Ono K, Lee K, Ideker T, Aza-Blanc P, Gleeson JG (2010). Functional genomic screen for modulators of ciliogenesis and cilium length. Nature 464, 1048–1051.

Kohli P, Höhne M, Jüngst C, Bertsch S, Ebert LK, Schauss AC, Benzing T, Rinschen MM, Schermer B (2017). The ciliary membrane-associated proteome reveals actin-binding proteins as key components of cilia. EMBO Rep 18, 1521–1535.

Liao J-C, Yang TT, Weng RR, Kuo C-T, Chang C-W (2015). TTBK2: a tau protein kinase beyond tau phosphorylation. Biomed Res Int 2015, 575170.

Lo C-H, Lin I-H, Yang TT, Huang Y-C, Tanos BE, Chou P-C, Chang C-W, Tsay Y-G, Liao J-C, Wang W-J (2019). Phosphorylation of CEP83 by TTBK2 is necessary for cilia initiation. J Cell Biol 218, 3489–3505.

Lopes CAM, Prosser SL, Romio L, Hirst RA, O'Callaghan C, Woolf AS, Fry AM (2011). Centriolar satellites are assembly points for proteins implicated in human ciliopathies, including oral-facial-digital syndrome 1. J Cell Sci 124, 600–612.

Loskutov YV, Griffin CL, Marinak KM, Bobko A, Margaryan NV, Geldenhuys WJ, Sarkaria JN, Pugacheva EN (2018). LPA signaling is regulated through the primary cilium: a novel target in glioblastoma. Oncogene 27, 1457–1471.

Loukil A, Barrington C, Goetz SC (2021). A complex of distal appendage-associated kinases linked to human disease regulates ciliary trafficking and stability. Proc Natl Acad Sci USA 118, 1–12.

Magistrati E, Maestrini G, Niño CA, Lince-Faria M, Beznoussenko G, Mironov A, Maspero E, Bettencourt-Dias M, Polo S (2021). Myosin VI regulates ciliogenesis by promoting the turnover of the centrosomal/satellite protein OFD1. EMBO Rep, 23, 1–19.

Mancini A, Sirabella D, Zhang W, Yamazaki H, Shirao T, Krauss RS (2011). Regulation of myotube formation by the actin-binding factor drebrin. Skelet Muscle 1, 1–13.

Melick CH, Jewell JL (2020). Regulation of mTORC1 by upstream stimuli. Genes 11, 1–28.

Mirvis M, Siemers KA, Nelson WJ, Stearns TP (2019). Primary cilium loss in mammalian cells occurs predominantly by whole-cilium shedding. PLoS Biol 17, e3000381.

Miyamoto T, Hosoba K, Ochiai H, Royba E, Izumi H, Sakuma T, Yamamoto T, Dynlacht BD, Matsuura S (2015). The microtubule-depolymerizing activity of a mitotic kinesin protein KIF2A drives primary cilia disassembly coupled with cell proliferation. Cell Rep 10, 664–673.

Nager AR, Goldstein JS, Herranz-Pérez V, Portran D, Ye F, Garcia-Verdugo JM, Nachury MV (2017). An actin network dispatches ciliary GPCRs into extracellular vesicles to modulate signaling. Cell 168, 252–263.e14.

Nakayama K, Katoh Y (2018). Ciliary protein trafficking mediated by IFT and BBSome complexes with the aid of kinesin-2 and dynein-2 motors. J Biochem 163, 155–164.

Odabasi E, Gul S, Kavakli IH, Firat-Karalar EN (2019). Centriolar satellites are required for efficient ciliogenesis and ciliary content regulation. EMBO Rep 20, 1–20.

Pigino G (2021). Intraflagellar transport. Curr Biol 31, R530–R536.

Pugacheva EN, Jablonski SA, Hartman TR, Henske EP, Golemis EA (2007). HEF1-dependent Aurora A activation induces disassembly of the primary cilium. Cell 129, 1351–1363.

Ran J, Yang Y, Li D, Liu M, Zhou J (2015). Deacetylation of α-tubulin and cortactin is required for HDAC6 to trigger ciliary disassembly. Sci Rep 5, 12917.

Sánchez I, Dynlacht BD (2016). Cilium assembly and disassembly. Nat Cell Biol 18, 711–717.

Seeley ES, Nachury MV (2010). The perennial organelle: assembly and disassembly of the primary cilium. J Cell Sci 123, 511–518.

Shu S, Liu X, Korn ED (2005). Blebbistatin and blebbistatin-inactivated myosin II inhibit myosin II-independent processes in *Dictyostelium*. Proc Natl Acad Sci USA 102, 1472–1477.

Singla V, Romaguera-Ros M, Garcia-Verdugo JM, Reiter JF (2010). Ofd1, a human disease gene, regulates the length and distal structure of centrioles. Dev Cell 18, 410–424.

Tang Z, Lin MG, Stowe TR, Chen S, Zhu M, Stearns T, Franco B, Zhong Q (2013). Autophagy promotes primary ciliogenesis by removing OFD1 from centriolar satellites. Nature 502, 254–257.

Tanos BE, Yang H-J, Soni R, Wang W-J, Macaluso FP, Asara JM, Tsou M-FB (2013). Centriole distal appendages promote membrane docking, leading to cilia initiation. Genes Dev 27, 163–168.

Wang G, Chen Q, Zhang X, Zhang B, Zhuo X, Liu J, Jiang Q, Zhang C (2013). PCM1 recruits Plk1 to the pericentriolar matrix to promote primary cilia disassembly before mitotic entry. J Cell Sci 126, 1355–1365.

Watanabe R, Wei L, Huang J (2011). mTOR signaling, function, novel inhibitors, and therapeutic targets. J Nucl Med 52, 497–500.

Watanabe T, Kakeno M, Matsui T, Sugiyama I, Arimura N, Matsuzawa K, Shirahige A, Ishidate F, Nishioka T, Taya S, et al. (2015). TTBK2 with EB1/3 regulates microtubule dynamics in migrating cells through KIF2A phosphorylation. J Cell Biol 210, 737–751.

Wollscheid H-P, Biancospino M, He F, Magistrati E, Molteni E, Lupia M, Soffientini P, Rottner K, Cavallaro U, Pozzoli U, et al. (2016). Diverse functions of myosin VI elucidated by an isoform-specific α-helix domain. Nat Struct Mol Biol 23, 300–308.